Lattices of double-quanta vortices and chirality inversion in $p_x + ip_y$ superconductors

Julien Garaud,[1,*] Egor Babaev,[1] Troels Arnfred Bojesen,[2] and Asle Sudbø[3]
[1]*Department of Theoretical Physics and Center for Quantum Materials, KTH-Royal Institute of Technology, Stockholm SE-10691, Sweden*
[2]*RIKEN Center for Emergent Matter Science, Wako, Saitama 351-0198, Japan*
[3]*Department of Physics, Norwegian University of Science and Technology, NO-7491 Trondheim, Norway*
(Received 13 May 2016; revised manuscript received 18 August 2016; published 13 September 2016)

We investigate the magnetization processes of a standard Ginzburg-Landau model for chiral p-wave superconducting states in an applied magnetic field. We find that the phase diagram is dominated by triangular lattices of doubly quantized vortices. Only in close vicinity to the upper critical field the lattice starts to dissociate into a structure of single-quanta vortices. The degeneracy between states with opposite chirality is broken in a nonzero field. If the magnetization starts with an energetically unfavorable chirality, the process of chirality inversion induced by the external magnetic field results in the formation of a sequence of metastable states with characteristic magnetic signatures that can be probed by standard experimental techniques.

DOI: 10.1103/PhysRevB.94.104509

I. INTRODUCTION

The complex structure of the order parameter for chiral p-wave superfluid and superconducting states has long attracted interest in the physical properties of said states. Chiral p-wave pairing is realized in the A-phase of superfluid ^{3}He, where the complex structure of the order parameter yields a rich variety of topological defects [1–6]. In the context of superconductivity, this interest is related to the discovery of Sr_2RuO_4 [7,8], which is argued to have p-wave pairing [9–11], with Cooper pairs having an effective internal orbital momentum [8,12].

Evidence supporting the existence of a chiral p-wave superconducting state in Sr_2RuO_4 has surfaced through a variety of measurements. For instance, the superconducting critical temperature (T_c) is completely suppressed by adding nonmagnetic impurities [7,8]. Moreover, NMR Knight shift measurements show no change in the spin susceptibility with temperature in the superconducting phase [13,14]. Muon spin measurements (μSR) [15] and the polar Kerr effect [16] suggest that the superconducting state breaks time-reversal symmetry. Also, phase-sensitive Josephson spectroscopy experiments have shown some evidence of a dynamic domain structure consistent with a chiral spin-triplet state [12,17]. Experiments on toroidal mesoscopic samples reporting magnetization with half-height steps suggest half-quantum vorticity [18], while no half-quantum vortices were reported in a singly connected geometry.

Nevertheless, the nature of the superconducting state of Sr_2RuO_4 remains elusive, since a number of properties predicted for chiral p-wave states have so far not been observed. Spontaneous breaking of time-reversal symmetry for a chiral p-wave state implies the existence of domain walls (DW) that separate two different time-reversal symmetry-broken (TRSB) ground states, i.e., different chiral states. As a consequence of broken spatial symmetry, these domain walls support spontaneous supercurrents that generate magnetic fields [19–23]. Edge currents are also expected to flow at the boundaries of samples, quite similarly to the currents at domain walls between domains of opposite chirality [21–24], and these currents will have a magnetic field associated with them. However, in Sr_2RuO_4, no indication of such a field has so far been found in magnetic imaging microscopy experiments [10,25–28]. Thus, the issue of identifying a possible model of the superconducting state in this compound is currently a matter of intense debate [24,29–35].

Vortex matter in Sr_2RuO_4 also shows rich physics that can give insight into the nature of a superconducting state in this material. The formation of chains of vortices has been reported for magnetic fields with an ab-plane component [36], consistent with the mechanism of vortex chain formation in layered systems. Small-angle neutron scattering [37] and muon-spin rotation measurements [38,39] have revealed vortex lattices with square symmetry at high fields. A transition to a triangular vortex lattice at lower fields has been reported in [39,40]. Such transitions of the vortex lattice structure have been regarded as being consistent with predictions based on lowest-Landau-level calculations for chiral p-wave superconductivity in Sr_2RuO_4 [41–43]. However, they are inconsistent with numerical studies of the energy of isolated topological defects [44] that have predicted the formation of double-quanta vortices in the Ginzburg-Landau model for a chiral p-wave superconductor. Early experiments also demonstrated "zero creep" that is not accompanied by a dramatic rise in critical current [45]. This indicates that vortices form relatively mobile clusters. The initial interpretation [45] of this experiment was taken as evidence for a chiral p-wave state that allows the formation of groups of type-2 vortices trapped by a closed chiral domain wall. Within this scenario, the domain wall would prevent vortex creep outside the sample. At the same time, in contrast to the vortex pinning scenario, these groups of vortices could be moved by an external current. This would explain the absence of a dramatic rise in the critical current. However, such a configuration would have characteristic magnetic signatures (see Refs. [44,46] and the discussion below). These signatures have not been seen so far in scanning surface probes. Instead, experiments using magnetic surface probes have reported observations of clusters of integer-flux vortices [25,27,47]. Evidence of vortex clustering has also been found in bulk measurements in field-cooled muon-spin

*garaud.phys@gmail.com

rotation experiments [39]. The key observation there was that vortex clusters contract as temperature is lowered well below T_c, which is inconsistent with vortex pinning. Reference [39] has attributed vortex coalescence to the competition between multiple coherence lengths that may originate from multiband effects or other multicomponent order parameters of various origins (such a "type-1.5" scenario was hypothesized in an earlier paper [27] in analogy with [48]).

In zero field, both chiral (ground) states are degenerate in energy, while this degeneracy is lifted by a magnetic field. For a given orientation of the magnetic field, only one of the chiral states is stable while the time-reversed chiral state is energetically penalized. Hence, the dominant component can form a vortex. Since the dominant component is suppressed in the vicinity of the vortex core, the time-reversed (subdominant) chiral component may be induced in the vortex core [43,49]. The winding of the induced component is not independent of that of the dominant component. It has a 4π winding of the relative phases that follows from the Cooper pairs having nonzero internal orbital momentum [50]. Since the magnetic field lifts the degeneracy between chiralities, vortices with opposite phase winding have different physical properties [44,49,51].

Apart from single-quanta vortices, there also exist stable vortices carrying multiple quanta of magnetic flux. These are essentially different from single-quanta vortices because as they are coreless, they carry an additional topological charge, and they are sometimes called skyrmions. As discussed in more detail below, the component induced by a doubly quantized vortex in the dominant component has zero winding [49,51]. The possible existence of lattices of double-quanta vortices has been proposed earlier in the context of the heavy-fermion compound UPt_3 [52,53], which is believed to be described by a similar type of model [54,55]. Based on self-consistent calculations using Eilenberger theory for the chiral p-wave state, it was recently argued that while lattices of single-quanta vortices form for fields close to H_{c1}, lattices of double-quanta vortices are favored in higher fields [56]. On the other hand, within the Ginzburg-Landau theory for chiral p-wave superconductors, double-quanta (coreless) vortices have been shown to be energetically favored as compared to two (isolated) single-quanta vortices [44], and they were also found to appear in a mesoscopic sample [57]. The energetic preference for double-quanta vortices does not exclude the formation of lattices of single-quantum vortices, or more complicated structures in a magnetization process. Interactions can favor different vortex lattices, or different Bean-Livingston barriers may result in the formation of metastable lattices for vortices that are not the most energetically favorable. This raises the question of the nature of magnetization processes and what kind of lattices form when an external magnetic field is applied.

In this paper, we investigate magnetization processes using numerical simulations of the minimal Ginzburg-Landau theory describing the chiral p-wave state in an external field directed along the **c** axis. In Sec. II, we introduce the Ginzburg-Landau theory used to describe the chiral p-wave state in an external field, and we discuss various basic properties, such as ground states and edge currents. Next, Sec. III is devoted to the magnetization process that has minimal energy, i.e., when the external field produces topological excitations with lowest energy. In that case, we find that lattices of double-quanta vortices are generically produced. Finally, Sec. IV investigates the magnetization processes with a reversed magnetic field. These states have higher energies and eventually lead to chirality inversion via a subtle interplay between vortices and domain walls.

II. GINZBURG-LANDAU MODEL

In the coordinate system in which the crystal anisotropy axis is $\mathbf{c} \parallel \mathbf{z}$, the $p_x + ip_y$ state corresponds to the two-dimensional representation $\Gamma_5^- = (k_x\mathbf{z}, k_y\mathbf{z})$ and the order parameter is described by a two-dimensional complex vector $\boldsymbol{\eta} = (\eta_x, \eta_y)/\sqrt{2}$ [8,55,58]. Introducing the chiral order parameter basis $\eta_\pm = \eta_x \pm i\eta_y$, the dimensionless Ginzburg-Landau free energy reads (see, e.g., [41–43])

$$\mathcal{F} = |\nabla \times \boldsymbol{A}|^2 + |\boldsymbol{D}\eta_+|^2 + |\boldsymbol{D}\eta_-|^2 \tag{1a}$$

$$+ (\nu+1)\mathrm{Re}[(D_x\eta_+)^* D_x\eta_- - (D_y\eta_+)^* D_y\eta_-] \tag{1b}$$

$$+ (\nu-1)\mathrm{Im}[(D_x\eta_+)^* D_y\eta_- + (D_y\eta_+)^* D_x\eta_-] \tag{1c}$$

$$+ 2|\eta_+\eta_-|^2 + \nu\,\mathrm{Re}(\eta_+^{*2}\eta_-^2) + \sum_{a=\pm} -|\eta_a|^2 + \frac{1}{2}|\eta_a|^4. \tag{1d}$$

Here $\eta_\pm = |\eta_\pm| e^{i\varphi_\pm}$ and we have used dimensionless units where the free energy is normalized to the condensation energy, and the lengths are given in units of $\xi = [\alpha_0(T - T_c)]^{-1/2}$. The magnetic field $\boldsymbol{B} = \nabla \times \boldsymbol{A}$ is given in units of $\sqrt{2}B_c = \Phi_0/(2\pi\lambda\xi)$. The dimensionless gauge coupling g that appears in the covariant derivative $\boldsymbol{D} = \nabla + ig\boldsymbol{A}$ is used to parametrize the ratio of two length scales in this Ginzburg-Landau model, $g^{-1} := \kappa = \lambda/\xi$. The anisotropy parameter ν, which satisfies $|\nu| < 1$, determines the anisotropy in the xy plane. It measures the tetragonal distortions of the Fermi surface, which has cylindrical geometry for $\nu = 0$, and it is defined as $\nu = (\langle v_x^4\rangle - 3\langle v_x^2 v_y^2\rangle)/(\langle v_x^4\rangle + \langle v_x^2 v_y^2\rangle)$ (where $\langle\cdot\rangle$ denotes the average over the Fermi surface). In the model defined by Eq. (1), the dependence on the third coordinate is not considered (i.e., assuming a two-dimensional system or translational invariance along the z axis). Varying Eq. (1) with respect to $\eta_\pm$ yields the Ginzburg-Landau equations given by

$$\Pi_{x^2+y^2}\eta_\pm + \left(\frac{\nu+1}{2}\Pi_{x^2-y^2} \pm \frac{\nu-1}{2i}\Pi_{xy}\right)\eta_\mp = \frac{\partial \mathcal{F}_p}{\partial \eta_\pm^*}$$

$$\text{with} \quad \Pi_{x^2\pm y^2} = D_xD_x \pm D_yD_y, \quad \Pi_{xy} = \{D_x, D_y\}, \tag{2}$$

where $\mathcal{F}_p$ is the potential term Eq. (1d) in the free energy, and $\{\cdot,\cdot\}$ stands for the anticommutator. Variation with respect to the vector potential gives Ampère's equation $\nabla \times \boldsymbol{B} + \boldsymbol{J} = \boldsymbol{0}$, where the total current is the sum of partial currents $\boldsymbol{J}^\pm$ whose components are

$$J_x^\pm = \frac{g}{2}\mathrm{Im}\left(\eta_\pm^*\left(D_x\eta_\pm + [D_\pm + \nu D_\mp]\frac{\eta_\mp}{2}\right)\right), \tag{3a}$$

$$J_y^\pm = \frac{g}{2}\mathrm{Im}\left(\eta_\pm^*\left(D_y\eta_\pm \pm i[D_\pm - \nu D_\mp]\frac{\eta_\mp}{2}\right)\right), \tag{3b}$$

where $D_\pm = D_x \pm iD_y$.

The theory described by Eq. (1) has several symmetries. First, Eq. (1) exhibits the usual U(1) gauge invariance under the transformation $\boldsymbol{\eta} \to e^{i\zeta(\boldsymbol{x})}\boldsymbol{\eta}$ and $\boldsymbol{A} \to \boldsymbol{A} - \boldsymbol{\nabla}\zeta(\boldsymbol{x})/g$. The theory is also invariant under a discrete ($\mathbb{Z}_2$) operation $\mathcal{T}$, which is referred to as time-reversal symmetry, $\{\eta_\pm, \boldsymbol{B}\} \xrightarrow{\mathcal{T}} \{\eta_\mp^*, -\boldsymbol{B}\}$. As discussed below, the chiral ground state spontaneously breaks this symmetry.

The nontrivial behavior of the superconducting degrees of freedom at the boundary of a sample is responsible for the generation of spontaneous edge currents. Within the Ginzburg-Landau theory, this behavior is accounted for by adding relevant surface terms of the form [58]

$$\mathcal{F}_{\text{surf}} = \left[\chi_1\left(n_x^2 + n_y^2\right) + \chi_z n_z^2\right]\left[|\eta_+|^2 + |\eta_-|^2\right] + 2\chi_2\left(n_x^2 - n_y^2\right)\text{Re}(\eta_+^*\eta_-) - 4\chi_3 n_x n_y \text{Im}(\eta_+^*\eta_-), \quad (4)$$

where $n_i \equiv \boldsymbol{n}\cdot\hat{\boldsymbol{\imath}}$ are the components of the normal vector to the boundary. In our two-dimensional problem, $\chi_z = 0$, and for simplicity we can choose $\chi_1 = \chi_2 = \chi_3 \equiv \chi$, imposing specular reflection on the boundary. The magnetization processes are thus described by the total (Gibbs) free energy over a domain Ω,

$$G = \int_\Omega \mathcal{F} - 2\boldsymbol{B}\cdot H\hat{\boldsymbol{z}} + \int_{\partial\Omega} \mathcal{F}_{\text{surf}}, \quad (5)$$

together with the conditions that $\boldsymbol{\nabla}\times\boldsymbol{A} = H\hat{\boldsymbol{z}}$ at the boundary $\partial\Omega$ of the domain. Here H denotes the strength of an external field.

A. Details of the numerics

To numerically minimize Eq. (5), the physical degrees of freedom $\eta_\pm$ and $\boldsymbol{A}$ are discretized using a finite-element framework [59–61]. First we construct a mesh being a regular partition of the spatial domain using a Deleaunay-Voronoi triangulation algorithm. In other words, the spatial domain is subdivided into a set of triangles (having similar area). Then, $\eta_\pm$ and $\boldsymbol{A}$ are expressed in terms of second-order Lagrange polynomials (polynomials of x,y up to second order) on each triangle. This means that on a given triangle, each of the six physical degrees of freedom of the problem ($\eta_\pm$, $\eta_\pm^*$, and $\boldsymbol{A}$) is parametrized by the six coefficients of the second-order interpolating polynomials (there are six independent coefficients for a second-order polynomial in two dimensions). The second-order Lagrange interpolation defines the six coefficients at vertices and midedges, for a total of $6\times 6 = 36$ numerical degrees of freedom per triangle. The overall accuracy of the construction is determined by the number of triangles that constitute the mesh, as well as the order of the interpolation method.

Now, within this finite-element framework, we use a nonlinear conjugate-gradient algorithm (see, e.g., Ref. [62]), which is iterated until the relative variations of the norm of the functional gradient with respect to all degrees of freedom are less than 10^{-8}.

In this work, we investigate magnetization processes and vortex structure formation due to an applied magnetic field on domains of finite size. We focus on characteristic states that appear during magnetization processes, and which should be experimentally observable. We therefore do not specifically focus on the question of which vortex lattice is a ground state in a given field in the thermodynamic limit. Precise answers to minimal energy structure in a thermodynamic limit would require a different approach. There are intrinsic limitations to characterize a lattice structure when working on finite domains. First of all, realizing perfectly ordered lattices typically requires a certain number of vortices given a certain area. Unfortunately, during magnetization processes, the number of vortices varies, and hence the appropriate number of vortices may not be realized. Moreover, unlike in periodic domains, the overall lattice structure is determined by more than just intervortex forces. The existence of Meissner currents flowing along boundaries can also alter the lattice structure. Although such effects should tend to be less important in very large domains, this explains why, in rather high fields, the structure we find can be distorted or less ordered.

B. Ground state

The ground state that minimizes the potential energy, Eq. (1d), is degenerate, and the solutions are $(\eta_+,\eta_-) = (1,0)$ and $(0,1)$. With regard to symmetry, it spontaneously breaks the $\text{U}(1)\times\mathbb{Z}_2$ symmetry, where $\mathbb{Z}_2$ refers to time-reversal operations. The spontaneous breakdown of the discrete $\mathbb{Z}_2$ symmetry dictates that the theory allows domain-wall solutions that interpolate between regions in different ground states. Such domain walls carry a magnetic field perpendicular to the xy plane [21,22]. Aspects of the domain-wall physics and their role in chirality switching are discussed later, in Sec. IV.

The discrete ($\mathbb{Z}_2$) degeneracy of the ground state is lifted for a nonzero applied field $H\hat{z}$. Consider, for example, a constant magnetic field induced by the external field $\boldsymbol{B} = B_z\hat{z} = H\hat{z}$. If $B_z > 0$, the ground state is $(\eta_+,\eta_-) = (1,0)$, while when $B_z < 0$, the lowest-energy state is $(\eta_+,\eta_-) = (0,1)$. As the η_+ and η_- components behave differently in an external field, a complete study for a given ground state necessitates considering both situations $B_z > 0$ and $B_z < 0$. Note that due to the time-reversal symmetry of the theory $\{\eta_\pm, \boldsymbol{B}\} \xrightarrow{\mathcal{T}} \{\eta_\mp^*, -\boldsymbol{B}\}$, this is equivalent to investigating only a fixed direction of the magnetic field (say $B_z > 0$), however including both chiral states. In the following, we choose to fix the dominant component of the order parameter to be η_- [i.e., the ground state is $(\eta_+,\eta_-) = (0,1)$], and thus we investigate both positive and negative applied magnetic fields.

C. Edge currents

Spontaneous currents are expected to appear at the boundaries of chiral p-wave superconducting samples. However, scanning Hall [25] and scanning SQUID microscopy [26,27] experiments in Sr_2RuO_4 have not detected such predicted edge currents, which in general should affect magnetization processes of chiral p-wave superconductors. If such edge currents are strong enough, the physics of vortex entry into the system can be substantially modified compared to that in ordinary superconductors. Indeed, as discussed in detail below, the edge current can affect the Bean-Livingston barrier and hence the processes of vortex entry. For example, it can

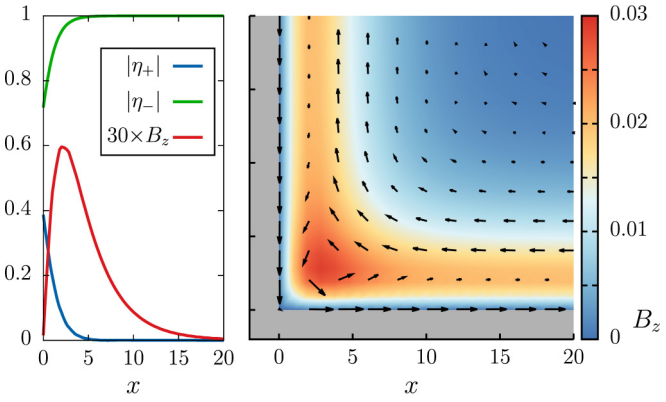

FIG. 1. Properties of the edge currents due to the surface term (4) for $\chi_1 = \chi_2 = \chi_3 = 1$. The left panel shows the behavior of the components $|\eta_\pm|$ and the magnetic field as a function of the distance from a straight edge boundary along the y axis. The right panel shows the circulating edge current and the induced magnetic field near a corner.

either facilitate or suppress vortex entry near H_{c1}, a fact that will affect the chirality inversion process.

The spontaneous magnetic field due to edge currents is found by minimizing Eq. (5) in zero external field ($H = 0$). Figure 1 shows that the spontaneous currents at the edges (here circulating counterclockwise) induce a magnetic field that is screened in the bulk by superconducting currents (here circulating clockwise). The calculation clearly shows that the magnetic field in the corner is enhanced as compared to a straight edge.

Note that the orientation of the edge currents is specified by the chirality of the superconducting state. For example, in Fig. 1 the dominant component is η_- and the currents circulate counterclockwise. In the case in which the dominant component is η_+, the currents circulate clockwise. In principle, the surface term, Eq. (4), responsible for the edge currents should not affect the bulk properties, such as, for example, vortex lattices. However, as discussed below, since the surface term modifies the boundary behavior, it can strongly influence vortex entry during a magnetization process and thus lead to qualitatively new features. In general, the boundary terms are important at low fields and have less of an influence at high fields.

III. LATTICES OF DOUBLE-QUANTA VORTICES

As stated above, the discrete degeneracy of the chiral ground state is lifted by an external field. This implies that given a ground state [which we take to be $(\eta_+,\eta_-) = (0,1)$], the magnetization processes will be different whether the applied field is parallel or antiparallel to the **c** axis. Similarly, vortices with counterclockwise winding have different energy than vortices with clockwise winding. After briefly reviewing the elementary properties of vortex matter in the theory of a chiral p-wave superconducting state, Eq. (1), we investigate the magnetization processes when $H < 0$, i.e., the case when an applied field excites vortices that have the least energy. This magnetization process is that of least energy, and it exhibits the formation of a triangular lattice of double-quanta vortices, which dissociates into a lattice of single-quanta vortices in the vicinity of the upper critical field H_{c2}.

A. Isolated vortices and skyrmions

The asymptotic vorticity of the dominant component η_- determines the sign of B_z, as well as the vorticity of the subdominant component η_+ [43], according to

$$\eta_- \propto e^{in_-\theta}, \quad \eta_+ \propto e^{in_+\theta}, \text{ and } n_+ = n_- + 2 \in \mathbb{Z}. \tag{6}$$

The relative phase φ_--φ_+ between the components η_+ and η_-, which corresponds to a difference $\Delta l = 2$ of the order parameters' angular momentum, originates with the structure of mixed gradients, Eqs. (1b) and (1c). Note that since the subdominant component, η_+, vanishes asymptotically (i.e., it recovers its ground-state value $\eta_+ = 0$ in the bulk phase), the winding n_+ can be located only in the close vicinity of a vortex core. Hence, the number of flux quanta is determined only by the winding number n_- of the dominant component. Equation (6) implies that the two possible single-quanta vortices are $(n_-,n_+) = (+1,+3)$ and $(n_-,n_+) = (-1,+1)$. Having different winding numbers of the subdominant component, these will have different core structures, and it is thus natural to expect that they will have different energies as well.

In agreement with the naive expectation, since it has a simpler core structure, the $(n_-,n_+) = (-1,+1)$ vortex can have a lower energy than the $(n_-,n_+) = (+1,+3)$ vortex [44,51]. As a result, the vortex with the lowest energy carries a magnetic field antiparallel to the **c** axis (for the case in which the dominant component is η_+, the lowest-energy vortex carries a magnetic field parallel to the **c** axis). The preference for the $(n_-,n_+) = (-1,+1)$ vortex, featuring the simpler core structure, occurs in the whole (ν,g) parameter space [at least within the Ginzburg-Landau model, Eq. (1)] [44]. It also follows that $(n_-,n_+) = (-1,+1)$ and $(n_-,n_+) = (+1,+3)$ have different lower critical fields, $H_{c1}^{(-1)} < H_{c1}^{(+1)}$. In other words, given a dominant component in the ground state, the first vortex entry occurs at different values of the applied field, according to whether it is parallel or antiparallel to the **c** axis [63,64].

The winding number n_- of the dominant component η_- specifies the topological sector. In infinite domains, different topological sectors are separated by an infinite energy barrier, which becomes finite (but still very high) in finite spatial domains. This implies a "topological protection" because no continuous finite-energy transformation can change the topological sector. As a result, a minimization algorithm that continuously deforms the field configurations to reduce the energy cannot change the number of flux quanta.[1] More precisely, starting with a configuration having a given winding n_-, the specifics of the minimization algorithm can affect core structures, but the asymptotic behavior of the vortices after convergence of the algorithm will, regardless of the algorithmic details, naturally behave as expected from Eq. (6).

[1]Note that this is rigorously true in infinite domains, while in finite domains there is the possibility to change the topological sector by entering/exiting topological defects (vortices) through the boundary of the domain.

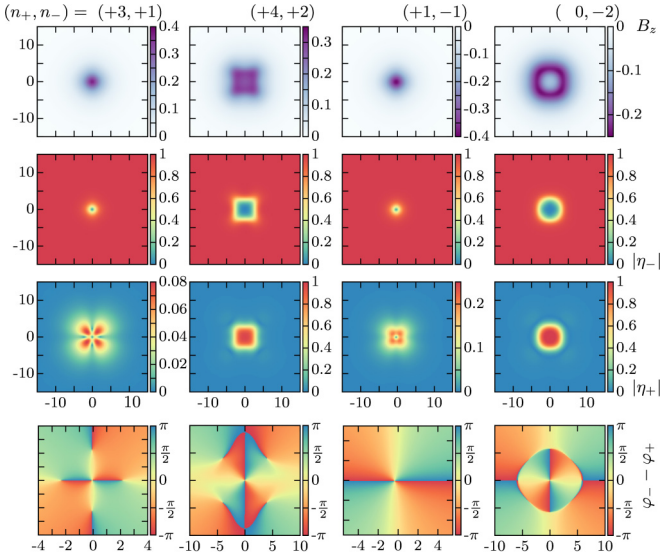

FIG. 2. Vortex states for the model defined in Eqs. (1) and (4) with parameters $g = 0.3$ and $\nu = 0.2$. The first line shows the magnetic field $\boldsymbol{B}$, while the second and third lines display η_- and η_+, respectively. The fourth line shows the relative phase φ_--φ_+ between η_+ and η_-. Winding the relative phase indicates the position of the cores of η_+ and η_-. The first two columns show single- and double-quanta vortices, respectively, with $B_z > 0$, while the third and fourth columns display single- and double-quanta vortices with $B_z < 0$.

The heuristic argument of the simplicity of the core structure of the vortices also implies the rather unusual situation that double-quanta vortices could be favored compared to two isolated single-quanta vortices [44,49,51,56,57]. Indeed, the double-quanta $(n_-,n_+) = (-2,0)$ vortex, as it has a simple core structure, is always energetically favored compared to two isolated single-quanta $(n_-,n_+) = (-1,+1)$ vortices [44]. Thus, one may expect the double-quanta vortices to form in an external field, at least close to H_{c1}. However, as they carry more flux, their entry through the boundary could be unlikely because they experience a different Bean-Livingston barrier.

Figure 2 illustrates the richness of the core structure of vortices. It is evident that vortices with opposite winding of the dominant component $n_- = \pm 1$ have different structures. In particular, the position and number of cores of the different components can be extracted from the last row, which shows the relative phase φ_--φ_+. Far from the cores, the components reach their asymptotic values $\varphi_\pm = n_\pm\theta$ given by Eq. (6). Thus, the relative phase φ_--φ_+ shows the expected 4π winding at large distances. Figure 2 also displays the two possible configurations carrying two flux quanta. Clearly, these also have different core structures. The $(n_-,n_+) = (-2,0)$ vortices are always less energetic than two isolated single-quanta vortices with $(n_-,n_+) = (-1,+1)$ (see Ref. [44] for a detailed analysis). Note that there also exist $(n_-,n_+) = (+2,+4)$ vortices. Their energy, compared to that of isolated $(n_-,n_+) = (+1,+3)$ vortices, can either be larger or smaller depending on the parameters (ν,g). In the regimes investigated here, the double-quanta $(n_-,n_+) = (+2,+4)$ vortices have higher energy than isolated ones. Thus, they are only metastable. Alternatively, the vortices discussed above can be understood as bound states of half-quantum vortices in term of the components (η_x,η_y) of the order parameter (see the corresponding discussion in Appendix). These (coreless) vortices carrying multiple flux-quanta can be characterized by additional topological invariants, motivating the alternate terminology of skyrmions [44].

B. Magnetization process—Lattices of double-quanta vortices

The physics of isolated vortices strongly suggests that double-quanta vortices should form in an external field. Here, we investigate the magnetization processes, starting from the Meissner state and ramping-up the applied field antiparallel to the **c** axis ($H < 0$). The solution in zero field is chosen to be the $(\eta_+,\eta_-) = (0,1)$ ground state. The external field is then sequentially increased (in steps of 4×10^{-3}), and the energy is minimized at each step. Figure 3 shows the outcome of such a magnetization process. This procedure corresponds to an applied field that, in the sense that it produces the less energetic defects, is optimally directed. As expected from the properties of the isolated vortices, the initial vortex entry comes in the form of double-quanta vortices. In our simulation, Fig. 3, the initial entry occurs at $|H| \simeq 0.46$. As the applied field increases, more double-quanta vortices enter and they arrange themselves in a regular lattice of double-quanta skyrmions. This lattice state is robust and persists for all applied fields. The preference for lattices of double-quanta vortices, in the case of an antiparallel external field, is a robust feature. We observed this behavior for all the parameters of the model we considered.

Since the strength of the edge currents depends on χ, the Bean-Livingston barrier for vortex entry is affected as well. We find that the entry of skyrmions occurs for a wide range of values of the parameter χ that parametrizes the edge properties. The value of the field for initial entry depends on the interplay with the edge currents. Nonetheless, bulk properties are essentially unaffected such that lattices of double-quanta vortices are always realized.

As stated earlier in more detail in Sec. II A, characterizing the lattice structure within our framework of working on a finite-size domain can be difficult. Due to uncontrollable vortex entry during the magnetization process and the interaction between vortices and Meissner currents flowing along the edge of the domain, perfect lattice structures are in practice never realized. Nonetheless, at least in rather low fields, it is quite clear that hexagonal lattices of two-quanta vortices are realized. In higher fields, the coexistence of a few single-quanta vortices distorts the overall structure, but the tendency to form a hexagonal lattice is nevertheless quite robust.

C. Lattice dissociation near H_{c2}

The results in Fig. 3 show the magnetization process from low to rather high fields when $H < 0$ is optimally directed. It is important to further understand the behavior in high fields near the second critical field H_{c2}. From the energetics of isolated vortices and from the magnetization processes, one would conclude that the double-quanta vortices are always favored for the model we consider. This would contradict earlier calculations using the lowest Landau-levels-based approach

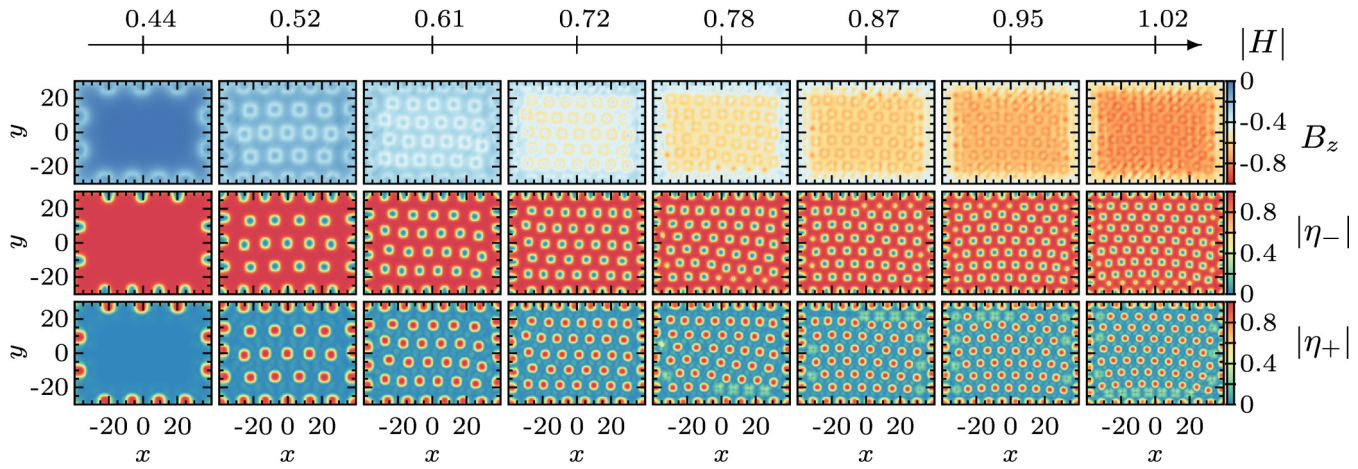

FIG. 3. Simulation in an external field $H < 0$ for the parameters $g = 0.3$, $\nu = 0.3$, and $\chi = 0.1$. The different lines display B_z, $|\eta_-|$, and $|\eta_+|$, respectively. Here, the orientation of the external field is such that it will produce less energetic topological defects (skyrmions). The panel corresponding to the lower field show half-quanta vortices stabilized near boundary. Increasing the field past H_{c1} produces entry of double-quanta vortices that arrange themselves into a hexagonal lattice. Note that in higher fields, both single- and double-quanta vortices enter the system. The single-quanta vortices will eventually merge into double-quanta skyrmions.

predicting that a square lattice of single-quanta vortices is the solution near H_{c2} [41,42].

To investigate the properties near H_{c2}, we need to slightly modify our parametrization of the theory, formulating it in a manner that is more convenient for numerical purposes.[2] The idea is that instead of approaching the upper critical field by varying H at fixed T in the (H,T)-phase diagram, the physics near H_{c2} can be found by varying T at fixed H. In mean-field theory, Eq. (1), the temperature dependence is absorbed by setting the scales of the problem (here temperature refers to the temperature parameter of the nonfluctuating mean-field theory). We restore the parametrization of the temperature dependence by having the prefactor of the quadratic terms in Eq. (1): $\alpha(\tilde{T}) = 1 - \tilde{T}$. Thus $\tilde{T} = 1$ corresponds to the destruction of the superconducting state in zero field. Decreasing the value of the parameter α will thus decrease the superconducting density and push the system toward H_{c2}.

Starting in the Meissner state with $\alpha = 1$, the external field is gradually increased. The resulting magnetization process, similar to that displayed in Fig. 3, produces a lattice of double-quanta vortices. Once the lattice is established, the applied field is fixed and the parameter α is sequentially decreased from 1 to 0 (in steps of 2.5×10^{-2}), and the energy is minimized at each step. Figure 4 shows the evolution of a vortex lattice when decreasing α toward H_{c2}. The system exhibits a lattice of double-quanta vortices for a rather wide range of temperatures.

[2]Approaching H_{c2} requires large fields, which can make numerical investigations difficult. Indeed, when applying higher fields, the domain is populated by more and more vortices. As a result, the complex fields have a larger and larger winding number at the boundary. Thus, in order to preserve reasonable accuracy (number of boundary points per winding number), one would need to refine the mesh, which would result in a dramatic slowdown of the numerics. Instead, horizontal displacement in the (H,T)-phase diagram allows us to approach H_{c2} without the special need to refine the mesh.

When getting closer to H_{c2}, the lattice starts to deform and the double-quanta vortices split into single-quanta vortices. Eventually, the entire lattice of double-quanta vortices has dissociated into a structure of single-quanta vortices. Because finite-size effects become important together with a longer equilibration time, it becomes very difficult to form a fully ordered state. Thus, it is difficult to rigorously characterize such a lattice structure (see the discussion in Sec. II A). However, we can infer that our results, together with the earlier results based on lowest Landau-level calculations [41,42], point toward a transition to a lattice of a single-quanta vortices. Structures obtained by lowest Landau-level calculations near H_{c2} are square lattices of the single-quanta vortices [41,42].

The difference with the previously discussed scenario is that our results indicate that square lattices of single-quanta vortices should transform into a hexagonal lattice of double-quanta vortices. The latter is robust and survives to large negative values of $H < 0$. Only in close vicinity to the upper critical field H_{c2} will double-quanta vortices dissociate. Note also that in the crossover region, single- and double-quanta vortices coexist, and there is a tendency to form vortex stripes.

IV. CHIRALITY INVERSION AND THE ROLE OF DOMAIN WALLS

The discrete degeneracy of the chiral ground state is lifted by an external field, and thus the magnetization processes should be different from that previously discussed when the applied field is parallel to the **c** axis. Magnetization processes when $H > 0$ imply that the system can be in metastable states that are not energetically optimal. Indeed, the Meissner state with an initial chirality that does not correspond to the optimal direction of the applied field is not the one with the lowest energy. Domain walls are natural topological excitations that interpolate between two ground states. In general, they are expected to form via a Kibble-Zurek-like mechanism [23], but they could also play a role in the magnetization process where

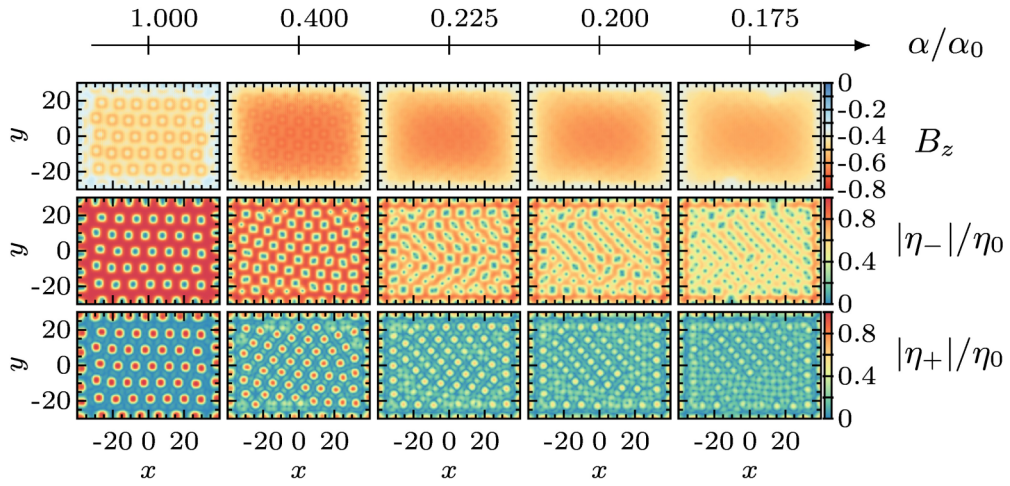

FIG. 4. Simulation in an external field $H < 0$ for the parameters $g = 0.3$, $\nu = 0.3$, and $\chi = 0.1$. The different lines display B_z, $|\eta_-|$, and $|\eta_+|$, respectively. Here, the external field is fixed and the prefactor of the quadratic term is varied, while other coefficients are kept fixed. This is equivalent to varying the temperature and getting closer to H_{c2}. The first panel corresponds to the last panel of Fig. 3. Decreasing α/α_0 decreases the total density. Close enough to H_{c2}, the double-quanta vortices start to break apart. Eventually, very close to H_{c2} only single-quanta vortices subsist, and they arrange themselves in a square lattice.

the starting state is not the optimal one in an external field. Various aspects of domain-wall properties during magnetization processes have been studied in [63,64]. After briefly reviewing their elementary properties, we investigate the magnetization processes when $H > 0$. This magnetization process is actually much richer than that taking place when the starting state is an optimal one in a given external field. Indeed, for nonoptimal starting states, we will discover that the magnetization process involves chirality inversion processes, the details of which will be sensitive to the parameters of the theory.

A. Domain walls

A domain wall is a field configuration that interpolates, for example, between $(|\eta_+|,|\eta_-|) = (1,0)$ and $(|\eta_+|,|\eta_-|) = (0,1)$. Note that there are two inequivalent ways of having such a configuration, with differing corresponding domain walls. The two inequivalent ways may be illustrated by

$$\mathrm{DW_I}\ :\quad (-1,0) \longleftarrow (\eta_+,\eta_-) \longrightarrow (0,1), \tag{7a}$$

$$\mathrm{DW_{II}}:\quad (\ \ 1,0) \longleftarrow (\eta_+,\eta_-) \longrightarrow (0,1). \tag{7b}$$

It is easily realized that the two domain-wall configurations cannot be transformed into each other by gauge transformations, from which they are physically distinguishable. Note that the energy cost of a domain wall also depends on its relative orientation with respect to the crystal axis. Depending on the orientation of the domain wall, one of the two possible domain walls is favored. This was discussed in detail in Ref. [65].

Figure 5 displays the typical domain-wall solution in chiral p-wave superconductors. The magnetic signatures of the two types of domain walls [Eq. (7)] are different, and they have different energies. Due to partial currents in different chiralities, the domain walls have longitudinal currents associated with them, and hence they carry a magnetic field, as can be seen from Fig. 5. Conversely, since the domain walls support longitudinal currents, an external applied field will produce a Lorentz force that should induce motion of the domain wall. In other words, when the degeneracy between ground states is lifted by an external field, the domain wall should move to increase the region of optimal ground state. Thus, we expect domain walls to be involved in the magnetization processes when the external field is not optimally oriented.

B. Chirality inversion in an external field

Domain walls are the topological excitations that are involved in processes that revert the chirality. For an applied

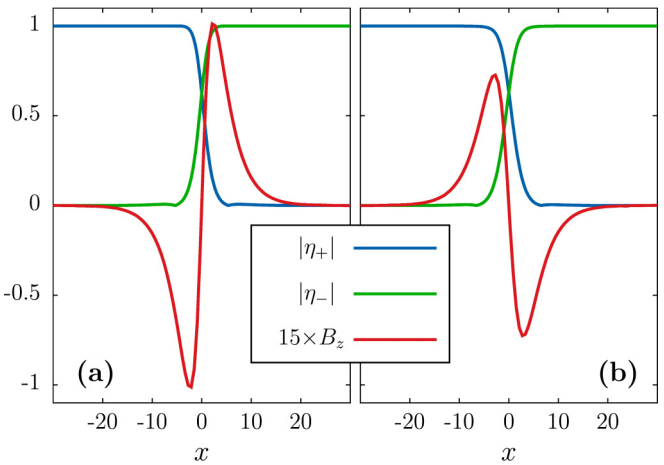

FIG. 5. The two possible kinds of domain walls interpolating between $(|\eta_+|,|\eta_-|) = (1,0)$ and $(|\eta_+|,|\eta_-|) = (0,1)$ for the parameters $g = 0.3$ and $\nu = -0.5$. Panels (a) and (b) show $\mathrm{DW_I}$ and $\mathrm{DW_{II}}$ domain walls, respectively. Their density profiles are very similar, but they differ from their real and imaginary parts and they cannot be transformed into each other. Although the density profiles are quite close to each other, the two domain walls have different energies and also different magnetic field due to the difference in the relative phases.

field parallel to the c axis ($H > 0$), the ground state $(\eta_+,\eta_-) = (0,1)$ is not the optimal one. Thus, two isolated single-quanta vortices have lower energy than a double-quantum vortex. That is, $(n_+,n_-) = (+3,+1)$ vortices have a smaller lower critical field than the double-quanta $(n_+,n_-) = (+4,+2)$ vortices, i.e., $H_{c1}^{(n_-=+1)} < H_{c1}^{(n_-=+2)}$. The top panel in Fig. 6 illustrates this, and only single-quanta vortices enter and organize as a lattice. Note that the field for the first vortex entry in this case is higher than for an antiparallel field, since $H_{c1}^{(n_-=+1)} > H_{c1}^{(n_-=-1)}$. Therefore, single-quanta vortices enter and arrange themselves as a lattice in a low field. An interesting process occurs in higher fields. Since the ground state $(\eta_+,\eta_-) = (0,1)$ is not optimal for that direction of the external field, the optimal case would thus actually be to have the opposite chirality. For rather large fields, we see that the system starts to "reverse" its chirality. By nucleating a domain wall that propagates from the boundaries, the system is able to switch to optimal chirality, given the orientation of the external field. While the domain wall propagates in the bulk, it "absorbs" the single-quanta vortices and "converts" them into double-quanta vortices in the optimal chirality. Eventually, mostly double-quanta skyrmions occupy the domain and should turn into a lattice of skyrmions.

During the process of chirality inversion, various kinds of vortices carrying different numbers of flux quanta can coexist. For instance, there are a few single-quanta vortices that are trapped between double-quanta vortices. They cannot always pair with other single-quanta vortices, as this would imply moving through the background of other double-quanta vortices. Such trajectories can be energetically unfavored. Similarly, skyrmions carrying more than two flux quanta are also formed and persist since these are metastable solutions. Their decay into double-quanta vortices can be triggered by the pressure that is exerted by the surrounding double-quanta skyrmions. We find that the skyrmions carrying high magnetic flux are eventually destroyed by an increasing field.

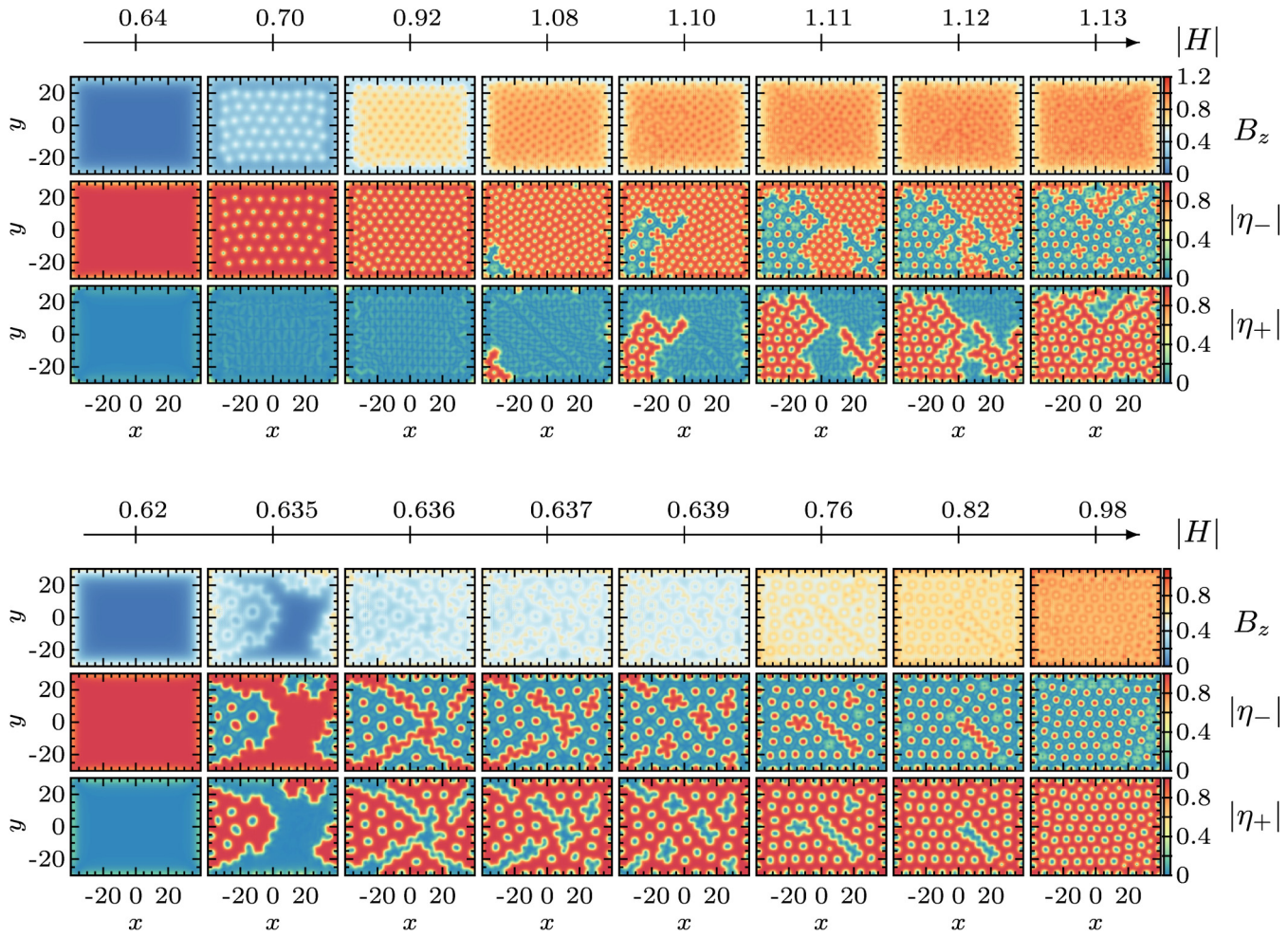

FIG. 6. Simulations in an external field $H > 0$ for the parameters $g = 0.3$ and $\nu = 0.15$. The different lines display B_z, $|\eta_-|$, and $|\eta_+|$, respectively. Here the orientation of the external field is such that it produces topological defects with higher energy: single-quanta (singular) vortices are favored over skyrmions. Given the direction of the applied field, the initial chirality is nonoptimal. The parameters of the edge currents χ are $\chi = 1$ for the top panel and $\chi = 10$ for the lower one. In the top panel, upon increasing the external field, single-quantum vortices enter and organize as a lattice. At elevated fields, a domain wall starts entering and "reverting" the chirality. In the lower panel, the domain wall starts entering the domain and switching the chirality before any vortex entry. The domain walls here also carry vorticity, as it becomes energetically beneficial to place vortices there. In both cases, behind the domain wall, the optimal chirality double-quanta skyrmions are the lowest-energy excitation. Eventually, mostly double-quanta skyrmions occupy the domain and should turn into a lattice of skyrmions.

Another possible scenario for the magnetization process with an external field parallel to the c axis is displayed in the lower panel of Fig. 6. Typically for small geometries, or for a strong barrier to vortex entries, it may be beneficial to produce a domain wall at a field below the lower critical field, and thus switch to the optimal chirality prior to any vortex entry. In addition to the domain wall, the optimal chirality double-quanta skyrmions are the lowest-energy excitations. The created domain walls are not the bare domain walls discussed above in Sec. IV A, but rather domain walls "decorated" by vortices, such that they carry vorticity. As a result of the vorticity that is trapped on the domain walls, they cannot easily annihilate (with an anti-DW), so they create skyrmions with a large number of flux quanta (see the details of the mechanism of stabilization of domain walls by vortex decoration in [44,46]). At elevated fields, however, these decorated domain walls eventually decay when the system is compressed enough, leaving a lattice of double-quanta vortices (in addition to a few isolated single quanta); the optimal chirality has been restored. From now on, the behavior of the double-quanta vortex lattice is the same as that discussed in Sec. III. That is, further increasing the external field will drive the structural transition into a single-quanta square lattice close to H_{c2}, accompanied by a density halving of the lattice.

We have found that a magnetic field antialigned with chirality should trigger a chirality inversion process by propagation of domain walls "decorated" with vortices inside the domain. We report two possibilities for such an inversion process, namely that domain-wall penetration occurs either before or after penetration of single-quanta vortices. Weak edge currents promote early entry of single-quanta vortices prior to the domain-wall penetration and chirality inversion process. Strong edge currents, on the other hand, delay entry of single-quanta vortices compared to the domain wall. In that case, the restoration of the optimal chiral state is much faster. Note that which of the two scenarios is realized depends not only on the strength of the edge currents, but also on the size and shape of the domain that is considered.

V. CONCLUSION

In this paper, we have considered the problem of magnetization of a finite superconducting sample in the framework of a standard Ginzburg-Landau model for chiral p-wave superconductors that is often invoked to describe Sr_2RuO_4. At magnetic fields close to H_{c2}, there is a tendency towards formation of a square lattice of single-quantum vortices, in agreement with earlier calculations [41,42] and experimental observations [37–39]. However, we find that, at least at mean-field level in the Ginzburg-Landau model, the square lattice exists only very close to H_{c2} and transforms into a hexagonal lattice of double-quanta vortices slightly below H_{c2}. This double-quanta hexagonal vortex lattice dominates the phase diagram of the model in question. In contrast to the Eilenberger theory-based calculations in Ref. [56], in our calculations the double-quanta vortex lattice persists down to the lowest fields. Double-quanta vortex formation has also been reported in simulations of mesoscopic samples in external fields [57].

Different chiralities are known to have different lower critical fields H_{c1}. For the chirality with larger H_{c1}, we have found metastable hexagonal vortex lattices of single-quanta vortices in low magnetic fields. The metastable single-quanta vortex lattices transform into a stable double-quanta vortex lattice at elevated fields via a set of complicated metastable states that involve the creation and growth of domain walls decorated by vortices. These metastable configurations have characteristic magnetic-field signatures that should be detectable by scanning SQUID and Hall probes or decoration.

Although our results are inconsistent with the current experimental data on Sr_2RuO_4 [25,27,39], they do not rule out p-wave superconductivity in this material. Rather, our results present evidence against a class of minimal models. This magnetization picture can be used as a "smoking gun" hallmark of chiral p-wave superconductivity that is searched for in other materials.

ACKNOWLEDGMENTS

We acknowledge fruitful discussions with Mihail Silaev. The work of J.G. and E.B. was supported by the Swedish Research Council Grant No. 642-2013-7837 and the Goran Gustafsson Foundation. The work of A.S. was supported by the Research Council of Norway Grants No. 205591/V20 and No. 216700/F20, as well as European Science Foundation COST Action MPI1201. The computations were performed on resources provided by the Swedish National Infrastructure for Computing (SNIC) at the National Supercomputer Center in Linköping, Sweden.

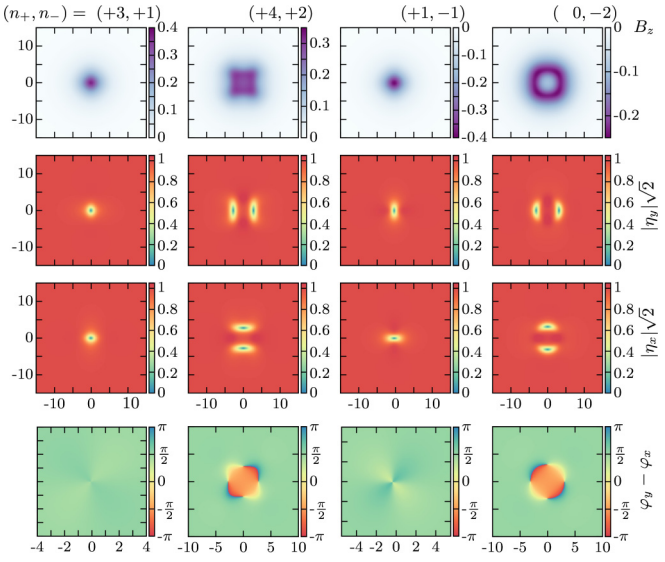

FIG. 7. Vortex states for the parameters $g = 0.3$ and $\nu = 0.2$. The first row shows the magnetic field $\boldsymbol{B}$, while the second and third row display η_y and η_x, respectively. The fourth line shows the relative phase φ_y-φ_x between η_x and η_y. The first two columns show single- and double-quanta vortices, respectively, with $B_z > 0$, while the third and fourth columns display single- and double-quanta vortices with $B_z < 0$.

APPENDIX: VORTICES IN TERMS OF $\eta_{x,y}$ COMPONENTS

It is instructive to consider the configurations displayed in Fig. 2 in the (η_x,η_y) order parameter basis, as is done in Fig. 7. There, the two inequivalent ground states have equal density and are distinguished by the relative phase φ_y-φ_x (between η_x and η_y) being $\pm\pi/2$. Again it is quite clear that opposite vorticities give different structures of the cores. The parametrization in terms of (η_x,η_y) sheds new light on how to interpret the double-quanta vortices. Since in this parametrization both η_x and η_y have nonzero ground-state density, both components can have nonzero (asymptotic) winding and thus contribute equally to screening of the magnetic field. A vortex within each component can be attributed half of a flux quantum, and a bound state of a half-quantum vortex in each component constitutes a single quantum vortex.

[1] N. D. Mermin and T.-L. Ho, Circulation and Angular Momentum in the *A* Phase of Superfluid Helium-3, Phys. Rev. Lett. **36**, 594 (1976).

[2] P. W. Anderson and G. Toulouse, Phase Slippage Without Vortex Cores: Vortex Textures in Superfluid ^{3}He, Phys. Rev. Lett. **38**, 508 (1977).

[3] P. M. Walmsley and A. I. Golov, Chirality of Superfluid ^{3}He $-A$, Phys. Rev. Lett. **109**, 215301 (2012).

[4] D. Vollhardt and P. Wolfle, *The Superfluid Phases of Helium 3*, Dover Books on Physics (Dover Publications, London, 2013).

[5] N. D. Mermin, The topological theory of defects in ordered media, Rev. Mod. Phys. **51**, 591 (1979).

[6] G. E. Volovik, *Exotic Properties of Superfluid* ^{3}He, Series in Modern Condensed Matter Physics (World Scientific, Singapore, 1992).

[7] Y. Maeno, H. Hashimoto, K. Yoshida, S. Nishizaki, T. Fujita, J. G. Bednorz, and F. Lichtenberg, Superconductivity in a layered perovskite without copper, Nature (London) **372**, 532 (1994).

[8] P. Mackenzie and Y. Maeno, The superconductivity of Sr_2RuO_4 and the physics of spin-triplet pairing, Rev. Mod. Phys. **75**, 657 (2003).

[9] T. M. Rice and M. Sigrist, Sr_2RuO_4: An electronic analog of ^{3}He? J. Phys.: Condens. Matter **7**, L643 (1995).

[10] C. Kallin and A. J. Berlinsky, Is Sr_2RuO_4 a chiral p-wave superconductor? J. Phys.: Condens. Matter **21**, 164210 (2009).

[11] C. Kallin, Chiral p-wave order in Sr_2RuO_4, Rep. Prog. Phys. **75**, 042501 (2012).

[12] K. D. Nelson, Z. Q. Mao, Y. Maeno, and Y. Liu, Odd-parity superconductivity in Sr_2RuO_4, Science **306**, 1151 (2004).

[13] H. Murakawa, K. Ishida, K. Kitagawa, Z. Q. Mao, and Y. Maeno, Measurement of the ^{101}Ru-Knight Shift of Superconducting Sr_2RuO_4 in a Parallel Magnetic Field, Phys. Rev. Lett. **93**, 167004 (2004).

[14] K. Ishida, H. Mukuda, Y. Kitaoka, K. Asayama, Z. Q. Mao, Y. Mori, and Y. Maeno, Spin-triplet superconductivity in Sr_2RuO_4 identified by 17O Knight shift, Nature (London) **396**, 658 (1998).

[15] G. M. Luke, Y. Fudamoto, K. M. Kojima, M. I. Larkin, J. Merrin, B. Nachumi, Y. J. Uemura, Y. Maeno, Z. Q. Mao, Y. Mori, H. Nakamura, and M. Sigrist, Time-reversal symmetry-breaking superconductivity in Sr_2RuO_4, Nature (London) **394**, 558 (1998).

[16] J. Xia, Y. Maeno, P. T. Beyersdorf, M. M. Fejer, and A. Kapitulnik, High Resolution Polar Kerr Effect Measurements of Sr_2RuO_4: Evidence for Broken Time-Reversal Symmetry in the Superconducting State, Phys. Rev. Lett. **97**, 167002 (2006).

[17] F. Kidwingira, J. D. Strand, D. J. Van Harlingen, and Y. Maeno, Dynamical superconducting order parameter domains in Sr_2RuO_4, Science **314**, 1267 (2006).

[18] J. Jang, D. G. Ferguson, V. Vakaryuk, R. Budakian, S. B. Chung, P. M. Goldbart, and Y. Maeno, Observation of half-height magnetization steps in Sr_2RuO_4, Science **331**, 186 (2011).

[19] G. E. Volovik and L. P. Gorkov, Superconducting classes in systems with heavy fermions, Zh. Eksp. Teor. Fiz. **88**, 1412 (1985) [J. Exp. Theor. Phys. **61**, 843 (1985)].

[20] M. Sigrist, T. M. Rice, and K. Ueda, Low-Field Magnetic Response of Complex Superconductors, Phys. Rev. Lett. **63**, 1727 (1989).

[21] M. Matsumoto and M. Sigrist, Quasiparticle states near the surface and the domain wall in a $p_x \pm ip_y$-wave superconductor, J. Phys. Soc. Jpn. **68**, 994 (1999).

[22] M. Matsumoto and M. Sigrist, Quasiparticle states near the surface and the Domain wall in a $p_x \pm ip_y$-wave superconductor, J. Phys. Soc. Jpn. **68**, 3120(E) (1999).

[23] V. Vadimov and M. Silaev, Predicted Nucleation of Domain Walls in $p_x + ip_y$ Superconductors by a Z_2 Symmetry-Breaking Transition in External Magnetic Fields, Phys. Rev. Lett. **111**, 177001 (2013).

[24] A. Bouhon and M. Sigrist, Current inversion at the edges of a chiral p-wave superconductor, Phys. Rev. B **90**, 220511 (2014).

[25] P. G. Björnsson, Y. Maeno, M. E. Huber, and K. A. Moler, Scanning magnetic imaging of Sr_2RuO_4, Phys. Rev. B **72**, 012504 (2005).

[26] J. R. Kirtley, C. Kallin, C. W. Hicks, E.-A. Kim, Y. Liu, K. A. Moler, Y. Maeno, and K. D. Nelson, Upper limit on spontaneous supercurrents in Sr_2RuO_4, Phys. Rev. B **76**, 014526 (2007).

[27] C. W. Hicks, J. R. Kirtley, T. M. Lippman, N. C. Koshnick, M. E. Huber, Y. Maeno, W. M. Yuhasz, M. B. Maple, and K. A. Moler, Limits on superconductivity-related magnetization in Sr_2RuO_4 and $PrOs_4Sb_{12}$ from scanning SQUID microscopy, Phys. Rev. B **81**, 214501 (2010).

[28] P. J. Curran, S. J. Bending, W. M. Desoky, A. S. Gibbs, S. L. Lee, and A. P. Mackenzie, Search for spontaneous edge currents and vortex imaging in Sr_2RuO_4 mesostructures, Phys. Rev. B **89**, 144504 (2014).

[29] S. Raghu, A. Kapitulnik, and S. A. Kivelson, Hidden Quasi-One-Dimensional Superconductivity in Sr_2RuO_4, Phys. Rev. Lett. **105**, 136401 (2010).

[30] Y. Imai, K. Wakabayashi, and M. Sigrist, Properties of edge states in a spin-triplet two-band superconductor, Phys. Rev. B **85**, 174532 (2012).

[31] S. Raghu, S. B. Chung, and S. Lederer, Theory of "hidden" quasi-1D superconductivity in Sr_2RuO_4, J. Phys.: Conf. Ser. **449**, 012031 (2013).

[32] N. A. Logoboy and E. B. Sonin, Domain walls in a tetragonal chiral p-wave superconductor, Phys. Rev. B **79**, 094511 (2009).

[33] T. Scaffidi and S. H. Simon, Large Chern Number and Edge Currents in Sr_2RuO_4, Phys. Rev. Lett. **115**, 087003 (2015).

[34] J. Garaud, D. F. Agterberg, and E. Babaev, Vortex coalescence and type-1.5 superconductivity in Sr_2RuO_4, Phys. Rev. B **86**, 060513 (2012).

[35] W. Huang, T. Scaffidi, M. Sigrist, and C. Kallin, Leggett modes and multiband superconductivity in Sr_2RuO_4, Phys. Rev. B **94**, 064508 (2016).

[36] V. O. Dolocan, P. Lejay, D. Mailly, and K. Hasselbach, Observation of two species of vortices in the anisotropic spin-triplet superconductor Sr_2RuO_4, Phys. Rev. B **74**, 144505 (2006).

[37] T. M. Riseman, P. G. Kealey, E. M. Forgan, A. P. Mackenzie, L. M. Galvin, A. W. Tyler, S. L. Lee, C. Ager, D. McK. Paul, C. M. Aegerter, R. Cubitt, Z. Q. Mao, T. Akima, and Y. Maeno, Observation of a square flux-line lattice in the unconventional superconductor Sr_2RuO_4, Nature (London) **396**, 242 (1998).

[38] C. M. Aegerter, S. H. Lloyd, C. Ager, S. L. Lee, S. Romer, H. Keller, and E. M. Forgan, Evidence for a square vortex lattice in Sr_2RuO_4 from muon-spin-rotation measurements, J. Phys.: Condens. Matter **10**, 7445 (1998).

[39] S. J. Ray, A. S. Gibbs, S. J. Bending, P. J. Curran, E. Babaev, C. Baines, A. P. Mackenzie, and S. L. Lee, Muon-spin rotation measurements of the vortex state in Sr_2RuO_4: Type-1.5 superconductivity, vortex clustering, and a crossover from a triangular to a square vortex lattice, Phys. Rev. B **89**, 094504 (2014).

[40] P. J. Curran, V. V. Khotkevych, S. J. Bending, A. S. Gibbs, S. L. Lee, and A. P. Mackenzie, Vortex imaging and vortex lattice transitions in superconducting Sr_2RuO_4 single crystals, Phys. Rev. B **84**, 104507 (2011).

[41] D. F. Agterberg, Vortex Lattice Structures of Sr_2RuO_4, Phys. Rev. Lett. **80**, 5184 (1998).

[42] D. F. Agterberg, Square vortex lattices for two-component superconducting order parameters, Phys. Rev. B **58**, 14484 (1998).

[43] R. Heeb and D. F. Agterberg, Ginzburg-Landau theory for a p-wave Sr_2RuO_4 superconductor: Vortex core structure and extended London theory, Phys. Rev. B **59**, 7076 (1999).

[44] J. Garaud and E. Babaev, Properties of skyrmions and multi-quanta vortices in chiral p-wave superconductors, Sci. Rep. **5**, 17540 (2015).

[45] E. Dumont and A. C. Mota, Unconventional vortex dynamics in superconducting states with broken time-reversal symmetry, Phys. Rev. B **65**, 144519 (2002).

[46] J. Garaud and E. Babaev, Skyrmionic state and stable half-quantum vortices in chiral p-wave superconductors, Phys. Rev. B **86**, 060514 (2012).

[47] V. O. Dolocan, C. Veauvy, F. Servant, P. Lejay, K. Hasselbach, Y. Liu, and D. Mailly, Observation of Vortex Coalescence in the Anisotropic Spin-Triplet Superconductor Sr_2RuO_4, Phys. Rev. Lett. **95**, 097004 (2005).

[48] V. Moshchalkov, M. Menghini, T. Nishio, Q. H. Chen, A. V. Silhanek, V. H. Dao, L. F. Chibotaru, N. D. Zhigadlo, and J. Karpinski, Type-1.5 Superconductivity, Phys. Rev. Lett. **102**, 117001 (2009).

[49] M. Ichioka and K. Machida, Field dependence of the vortex structure in chiral p-wave superconductors, Phys. Rev. B **65**, 224517 (2002).

[50] J. A. Sauls, A theory for the superconducting phases of UPt_3, J. Low Temp. Phys. **95**, 153 (1994).

[51] J. A. Sauls and M. Eschrig, Vortices in chiral, spin-triplet superconductors and superfluids, New J. Phys. **11**, 075008 (2009).

[52] Y. S. Barash and A. S. Mel'Nikov, Possible existence of nonsingular-vortex in UPt_3, Zh. Eksp. Teor. Fiz. Pis'ma Red. **51**, 511 (1990) [JETP Lett. **51**, 577 (1990)].

[53] A. S. Mel'nikov, Phase transitions in vortex lattices of hexagonal exotic superconductors, Zh. Eksp. Teor. Fiz. **101**, 1978 (1992) [J. Exp. Theor. Phys. **74**, 1059 (1992)].

[54] R. Joynt, Nature of the lower superconducting transition in UPt_3, Europhys. Lett. **16**, 289 (1991).

[55] R. Joynt and L. Taillefer, The superconducting phases of UPt_3, Rev. Mod. Phys. **74**, 235 (2002).

[56] M. Ichioka, M. Machida, and J. A. Sauls, Vortex states of chiral p-wave superconductors, J. Phys.: Conf. Ser. **400**, 022031 (2012).

[57] V. Fernández Becerra, E. Sardella, F. M. Peeters, and M. V. Milošević, Vortical versus skyrmionic states in mesoscopic p-wave superconductors, Phys. Rev. B **93**, 014518 (2016).

[58] M. Sigrist and K. Ueda, Phenomenological theory of unconventional superconductivity, Rev. Mod. Phys. **63**, 239 (1991).

[59] F. Hecht, New development in freefem++, J. Numer. Math. **20**, 251 (2012).

[60] D.V. Hutton, *Fundamentals of Finite Element Analysis*, Engineering Series (McGraw-Hill, New York, 2003).

[61] J. Reddy, *An Introduction to the Finite Element Method* (McGraw-Hill, New York, 2005).

[62] J. Nocedal and S. J. Wright, *Numerical Optimization*, 2nd ed., Springer Series in Operations Research (Springer, New York, 1999).

[63] Y. Matsunaga, M. Ichioka, and K. Machida, Vortex State in Double Transition Superconductors, Phys. Rev. Lett. **92**, 157001 (2004).

[64] M. Ichioka, Y. Matsunaga, and K. Machida, Magnetization process in a chiral p-wave superconductor with multidomains, Phys. Rev. B **71**, 172510 (2005).

[65] A. Bouhon and M. Sigrist, Influence of the domain walls on the Josephson effect in Sr_2RuO_4, New J. Phys. **12**, 043031 (2010).